ACS Biomaterials
SCIENCE & ENGINEERING

Article

Continuous Formation of Ultrathin, Strong Collagen Sheets with Tunable Anisotropy and Compaction

Shashi Malladi,[∇] David Miranda-Nieves,[∇] Lian Leng, Stephanie J. Grainger, Constantine Tarabanis, Alexander P. Nesmith, Revanth Kosaraju, Carolyn A. Haller, Kevin Kit Parker, Elliot L. Chaikof,* and Axel Günther*

Read Online

ACCESS | Metrics & More | Article Recommendations | SI Supporting Information

ABSTRACT: The multiscale organization of protein-based fibrillar materials is a hallmark of many organs, but the recapitulation of hierarchal structures down to fibrillar scales, which is a requirement for withstanding physiological loading forces, has been challenging. We present a microfluidic strategy for the continuous, large-scale formation of strong, handleable, free-standing, multicentimeter-wide collagen sheets of unprecedented thinness through the application of hydrodynamic focusing with the simultaneous imposition of strain. Sheets as thin as 1.9 μm displayed tensile strengths of 0.5−2.7 MPa, Young's moduli of 3−36 MPa, and modulated the diffusion of molecules as a function of collagen nanoscale structure. Smooth muscle cells cultured on engineered sheets oriented in the direction of aligned collagen fibrils and generated coordinated vasomotor responses. The described biofabrication approach enables rapid formation of ultrathin collagen sheets that withstand physiologically relevant loads for applications in tissue engineering and regenerative medicine, as well as in organ-on-chip and biohybrid devices.
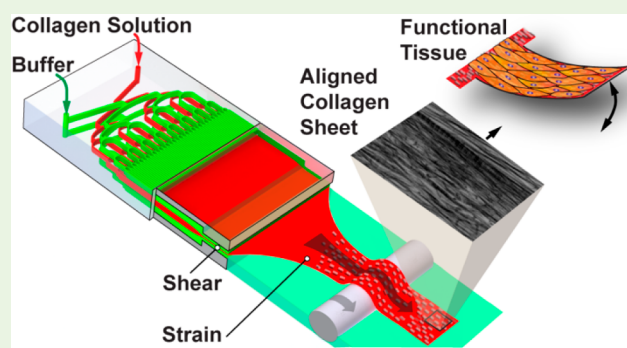
1. INTRODUCTION

The hierarchical organization of protein-based fibrillar materials is tissue specific and plays an important role in organ function. Collagen, the most abundant extracellular matrix (ECM) protein, accounts for up to 30% of the total protein mass in mammals, and its hierarchical organization in tissues is well studied.[1−3] Fibril-forming collagens are composed of right-handed triple helices that self-assemble through an entropy-driven process, known as fibrillogenesis, into fibrils, and, subsequently, combine to form collagen fibrils with diameters that range from 10 to 300 nm and a D-periodic banding pattern with a characteristic length scale of 54−67 nm.[2] The higher order organization of collagen fibrils varies between tissues and is closely linked to functional tissue characteristics. For example, in tendons, collagen fibrils, with a diameter distribution of 60 to 175 nm, are grouped into hierarchically organized and highly compacted fiber bundles that allow for the transmission of forces between bone and muscle tissue.[4,5] In the corneal stroma, unidirectionally aligned narrow fibrils with diameters of 31−34 nm stack to form 2-μm thin, transparent lamellae,[6,7] and within the wall of blood vessels, collagen fibrils with diameters of 30−100 nm are arranged into circumferentially aligned fibers with characteristic pitch angles of 18.8−58.9° for human aorta[2] that result in

increased ultimate tensile strength of the vascular wall and tolerance to physiological blood pressures.[8,9] See Table S1 for a summary of the mechanical and nanostructural properties of selected native tissues.

Efforts aimed at recapitulating tissue-specific multiscale organization of collagen remain limited. While 3D printing strategies have attempted to mimic collagen distribution at length scales between tens of microns and several centimeters,[10−12] to date, these approaches lack local control over fibril alignment and fibril packing density. As a result, these synthetic constructs are, in many cases, mechanically inferior to native tissues and often yield thick and loose structures.[13,14] Furthermore, strategies directed at inducing collagen fibril alignment have been largely limited to either shear-induced orientation of collagen within microfibers through wet spinning[15−19] or other approaches,[20,21] or induced alignment

within substrate-supported thin films by shear stress[22] or application of magnetic fields.[23] Free-standing collagen sheets have been produced by casting,[24,25] electrophoretic deposition,[26] or plastic compression;[27,28] affording films of disordered fibril structure, typically tens to hundreds of microns in thickness. The approach reported herein is the first strategy that affords the continuous formation of ultrathin, floating, highly aligned, dense collagen sheets at relevant length-scales and macroscale properties, which permit these sheets to be easily handled and manipulated.

2. MATERIALS AND METHODS

2.1. Isolation and Purification of Monomeric Collagen. Acid-soluble, monomeric rat-tail tendon collagen (MRTC) was obtained from Sprague−Dawley rat tails following Silver and Trelstad.[29] Frozen rat tails (Pel-Freez Biologicals, Rogers, AK) were thawed at room temperature and tendon was extracted with a wire stripper, immersed in HCl (10 mM, pH 2; 150 mL per tail) and stirred for 4 h at room temperature. Soluble collagen was separated by centrifugation at 30,000g and 4 °C for 30 min followed by sequential filtration through 20, 0.45, and 0.2 μm membranes. Addition of concentrated NaCl in HCl (pH 2) to a net salt concentration of 0.7 M, followed by 1 h stirring and 1 h centrifugation at 30,000g and 4 °C, precipitated the collagen. After overnight redissolution in HCl (10 mM) the material was dialyzed against phosphate buffer (20 mM) for at least 4 h at room temperature. Subsequent dialysis was performed against phosphate buffer (20 mM) at 4 °C for at least 8 h, and against HCl (10 mM) at 4 °C overnight. The resulting MRTC solution was frozen and lyophilized.

2.2. Preparation of Collagen Solution, Flow Focusing Buffer (FFB), and Fibrillogenesis Promoting Buffer (FPB). A collagen solution (5 mg/mL) was prepared by dissolving the lyophilized Type I monomeric collagen in deionized water (pH 2) containing blue food dye (Club House, Canada) for visualization. The solution was stirred continuously at 4 °C for 24 h to obtain an acidic collagen solution. The rapid gelation of collagen solution was induced by the addition of the buffering salts and polyethylene glycol (PEG), a molecular crowding and gelation triggering agent, to deionized water. The flow focusing buffer (FFB) comprised a neutralization buffer, which contained PEG (10 wt %, MW 35 kDa, Sigma-Aldrich), monobasic sodium phosphate (4.14 mg/mL, Sigma-Aldrich), dibasic sodium phosphate (12.1 mg/mL, Sigma-Aldrich), TES (6.86 mg/mL, Sigma-Aldrich), and sodium chloride (7.89 mg/mL, Sigma-Aldrich). The pH of the solution was adjusted to 8.[15] Following formation, collagen sheets were incubated in phosphate buffer to induce fibrillogenesis. The fibrillogenesis promoting buffer (FPB) was prepared in deionized water and consisted of sodium chloride (7.89 mg/mL), dibasic sodium phosphate (4.26 mg/mL), and Tris (10 mM), and the pH was adjusted to 7.4.[17]

2.3. Microfluidic Device Fabrication. The microfluidic devices were fabricated using multilayer soft lithography similar to a previously described process.[30] Briefly, two bifurcated microchannel networks were designed using computer-aided design software (AutoCAD, Autodesk, Mill Valley, CA, U.S.A.) for the distribution of the acidic collagen solution (red color, Figure S1) and the FFB solution (green color, Figure S1). The two corresponding hard masks were prepared using a desktop mask writer (Heidelberg uPG 501, Heidelberg Instruments, Heidelberg, Germany). The negative resist SU8−2050 (MicroChem, Newton, MA, U.S.A.) was spin coated in two subsequent steps onto a single-sided polished silicon wafer (3″, Wafer World, West Palm Beach, FL, U.S.A.). Briefly, a 75 μm-thick layer of resist was spin coated and prebaked for 6 min at 65 °C and for 15 min at 95 °C. Another 75 μm-thick layer was spun, baked 10 min at 65 °C, and for 35 min at 95 °C. Microchannel features were patterned by exposing the photomasks using a mask aligner (OAI model 30, UV power: 18.8 mW/cm²) for 13.3 s. The exposed substrate was post baked for 1 min at 65 °C and for 20 min at 95 °C and then developed in SU8 developer (MicroChem) for 12 min. The

three feature layers were first molded individually in polydimethylsiloxane (PDMS; Sylgard 184, Dow Corning, Midland, MI, USA) from the respective masters to define bifurcated microchannel networks with a uniform depth of 150 μm, and then vertically bonded on top of each other. The top and the bottom layers were identical, and served to distribute the buffer solution. The middle layer served to distribute the acidic collagen solution. The top layer was molded to be 3 mm thick and completely cured in an oven at 80 °C for 20 min. For the preparation of the middle layer, PDMS was spun to a thickness of 500 μm, partially cured, bonded to the top layer, and then completely cured.[31] The inlet hole to the second layer was defined using a 1.5 mm diameter biopsy punch (World Precision Instruments, Sarasota, FL, U.S.A.). The same process was repeated for the third layer. A through hole of 1.5 mm diameter was then punched through the first and third layers together. The three-layered device assembly was then sealed using blank thick layer (3 mm) using handheld Corona Treater (model BD-20, Electro-Technic Products, Chicago, IL, U.S.A.). The multilayered device was cured at 80 °C overnight, and PEEK tubing (1/16″ O.D. and 0.04″ I.D., Idex, Oak Harbor, WA, U.S.A.) was connected to the inlets using epoxy glue (Lepage Speed Set epoxy; Henkel Canada, Mississauga, ON, Canada). The device was cut at the outlet at a distance of 1 mm from the channel exit to expose the channels.

2.4. Aligned Collagen Sheet Formation. The formation of collagen sheets consisted of the co-extrusion of an acidic type I collagen and FFB solutions through a microfluidic device. First, the extrusion reservoir was filled with FFB such that the volume reached the center of the mandrel cross-sectional area. Then, rat tail type I collagen, pre-dissolved in deionized water (pH 2) at a concentration of 5 mg/mL, and FFB were injected into a three-layered microfluidic device (described above) at a flow rate of 400 μL/min and 4000 μL/min, respectively, using Tygon PVC clear tubing (1/16″ ID, 1/8″ OD, McMaster Carr, CA, U.S.A.), disposable plastic syringes, and two infusion pumps (model PHD 2000, Harvard Apparatus, Holliston, MA, U.S.A.). At the device outlet, the emerging collagen sheet was first manually guided through the bottom half of the constriction bracket and placed over the computer-controlled mandrel, followed by closure of the constriction bracket and initiation of mandrel rotation. Tweezers were used to maintain a floating sheet by preventing wrapping around the mandrel and tangling. Once the desired sheet length was achieved the rotating mandrel was stopped, and the sheet was manually cut from the segment extruded during startup. The resulting ultrathin collagen sheet was incubated in the FFB-filled reservoir for 30 min after extrusion, at which point it was washed 3× with deionized water and transferred to fibrillogenesis promoting buffer (FPB) for a 48 h incubation at 37 °C. Approximately, 500 μL was required to prime the system, that is, to generate a collagen sheet and position it over the mandrel. Once set up, 1 mL of acidic collagen solution resulted in a 70 cm long sheet.

Quantification of extruded sheet properties was conducted as a function of the dimensionless velocity

$$V^* = \frac{V_P - V_T}{V_T}$$

(1)

where

$$V_T = \frac{Q_B + Q_C}{W_0 H_C}$$

(2)

is the total bulk velocity of the solutions passing through the flow constriction, V_p is the velocity of the rotating mandrel, Q_B is the total flow rate of the FFB solution, 4000 μL/min, Q_C is the flow rate of the collagen solution, 400 μL/min, $W_0 = 35$ mm is the width of the exit section of the microfluidic device, and $H_C = 1$ mm is the height of the geometric constriction.

2.5. Sheet Thickness and Width Measurement. Collagen sheets were incubated for 1 h at room temperature in fluorescein isothiocyanate-dextran solution and washed thrice with deionized water. Samples were spread on coverslips (No. 1, thickness = 0.13 mm, width and length = 22 mm, Fisherfinest Premium superslip) and

imaged using either a Zeiss 710 or Nikon A1 inverted confocal laser scanning microscope with a 40× oil immersion objective (NA = 1.30, depth of field = 0.25 μm, and field of view = 250 μm × 250 μm) in the FITC channel (excitation: 490 nm, emission: 520 nm). Sheet thickness was determined by obtaining Z-stack image slices with a step size of 0.1 μm with analysis using a custom ImageJ macro. The selection of confocal pinhole and z-step size was determined based on values optimal for the objective selected. The collagen sheet thickness was calculated by averaging the thickness at every z-point across the stack, which was calculated by subtracting the threshold value from the maximum intensity. Confocal images with x−y tiling and 10% overlap were analyzed in ImageJ to determine sheet width.

2.6. FTIR Measurement. To confirm the absence of residual polyethylene glycol (PEG) within the collagen sheet or any chemical cross-linking induced by FFB, the sheets were characterized using a Fourier-transform Infrared (FTIR) spectrometer (model Vertex 70, Bruker Corp., Billerica, MA, U.S.A.). The sheets were pulverized and placed on the surface of a diamond ATR crystal (MIRacle, Pike Technologies, Madison, WI, U.S.A.) to obtain the end group peaks as a function of the wavenumber. The spectra of FFB and collagen solution were determined as baselines.

2.7. Strain Conditioning of Collagen Sheets. After extrusion, collagen sheets were incubated in FFB for 30 min and subsequently strain conditioned on a custom-made setup (Figure S4). The setup included two clamps, one fixed and a moveable clamp with a slider on opposing ends to secure the sheet firmly. The moveable clamp allowed the application of the desired strain rates. The setup also consisted of a reservoir that allowed collagen sheets to remain hydrated and submerged in fibrillogenesis promoting buffer (FPB) during the incubation period (48 h). Sheets were supported on an elastic polymer strip (Mold Star 30, Smooth-On, Macungie, PA, U.S.A.) that was molded within an acrylic frame and was 150 mm long, 20 mm wide, and 1.5 mm thick. Plasma treatment of the molded elastomeric support substrate for 90 s rendered the surface hydrophilic and allowed collagen sheets to readily spread. Mounting the sheet on the strain conditioning setup took around 10 min. After strain conditioning for 48 h at 37 °C, the collagen sheets were washed with deionized water, dried, and rehydrated prior to tensile testing.

2.8. Mechanical Testing. The axial and transverse tensile properties of rehydrated collagen sheets were measured using a Dynamic Mechanical Thermal Analyzer V (DMTA V, Rheometric Scientific, Piscataway, NJ, U.S.A.), with a 15 N load cell in the inverted orientation to facilitate hydrated measurements.[18] Briefly, collagen sheets were cut into rectangular pieces (10 mm × 20 mm) in the x and y directions, and immersed in PBS at 37 °C for 15 min. Before testing, samples were preconditioned by 15 cycles up to 66% of the average maximum failure strain. Testing consisted of straining at 4 mm/min until fracture. The elastic modulus, ultimate tensile strength, and strain-to-failure were determined from the stress−strain curve and the sheet dimensions (i.e., length, width, and thickness). Results were validated using a custom instrument as described by Tremblay et al.[32] Briefly, as described by Hakimi et al.,[33] samples were attached to custom C-shaped clamps, mounted on manual translation stages (MT1B, Thorlabs, Newton, U.S.A.), and pulled at speed of 0.01 mm/ s by a linear voice coil motor (LVCM-051-05-01, MotiCont, Van Nuys, CA, U.S.A.). A motion controller (DMC-4143, Galil, Rocklin, CA, U.S.A.) operated by a custom LabVIEW software program (National Instruments, Austin, U.S.A.) controlled the displacement of the voice coil motors. A load cell (model 31 Low, Honeywell, Charlotte, USA) was used to measure the force experienced at a given displacement, which was transferred to the motion controller using a DAQ card (USB-1208LS, Measurement Computing, Contoocook, NH, U.S.A.) and an amplifier (model UV-10, Honeywell, Columbus, OH, U.S.A.).

2.9. Transmission Electron Microscopy. Dry collagen sheets were washed thrice in cacodylate buffer (0.1 M) at pH 7.4 and fixed in glutaraldehyde (2.5%) and paraformaldehyde (2%) in cacodylate buffer (0.1 M) at pH 7.4 for 90 min. The samples were then washed again three times in cacodylate buffer (0.1 M) at pH 7.4 and with deionized water. Samples were then fixed with osmium tetraoxide

(1%) in cacodylate buffer (0.1 M) at pH 7.4 for 1 h. *En bloc* staining was done using uranyl acetate (2%) in deionized water for 1 h. Samples were again washed in deionized water, dehydrated in a series of ethanol solutions (25−100%), and then embedded in Quetol/ Spurr resin at 30% overnight, 67% for 8 h, 100% overnight, and polymerized in an oven at 60 °C for 48 h. Post-staining was done with uranyl acetate (5%) for 15 min, followed by Reynolds lead citrate for 15 min. Throughout the aforementioned processing steps, the sheet was sandwiched between two rectangular, centrally slotted PEEK pieces to ensure that a well-defined sheet orientation (flat, without wrinkles or folds) was maintained. The resin-embedded sheet within the central slot was cut out with a scalpel and 60−80 nm thin sections were cut with a microtome (model Leica Ultracut RMC MT-6000, Leica Mikrosysteme, Vienna, Austria). Sectioned samples were imaged using a transmission electron microscope (voltage 120 kV, TEM model Tecnai 20, FEI, Hilsboro, OR, U.S.A.).

2.10. Fibril Diameter, Density, Spacing, and Angular Alignment Quantification. Individual fibril diameters were obtained from TEM images for different V^* values using Nikon's NIS Elements Advanced Research (AR) Software (Version 4.13, Nikon Instruments, Melville, NY, U.S.A.). Each data point represents an average value of five images and at least 15 fibrils per image. Collagen fibril density was calculated by dividing the sum of collagen fibril area in a TEM image by the total image area. An autocorrelation function was calculated for the intensity distributions in the TEM images using "autocorr and acf" functions in Matlab (Mathworks, Econometrics Toolbox, Natick, MA, U.S.A.). The peak-to-peak distance between two adjacent peaks from the resulting plots was calculated to determine the fibril-to-fibril spacing. Lastly, the TEM images were converted to binary images, a fast Fourier transform (FFT) algorithm was applied to an oval profile, and "radial sum" analysis was conducted over 180 points in ImageJ. The data was shifted by 90° to obtain a central frequency peak for plotting the percentage of aligned fibrils as frequency (%) as a function of the angle of alignment. Full-Width-at-Half-Maximum (FWHM) was calculated from the difference between angles of alignment at which the frequency of alignment was half.

2.11. Fluorescence Recovery After Photobleaching (FRAP) Assay. Directionally dependent diffusivity, D, was measured within aligned collagen sheets by Fluorescence Recovery After Photo-bleaching (FRAP). Briefly, collagen sheets were incubated in Rhodamine 6G (R6G, 10 mM, M_w = 479.01 g/mol, Sigma-Aldrich) and fluorescein dextran (FITC, 15 μM, M_w = 150 000 g/mol, Sigma-Aldrich) solutions prepared in glycerol/water buffer. Stained collagen sheets were transferred and spread uniformly on 100 μm-thick coverslips (Ted Pella Inc.) and inspected on an inverted confocal microscope (Nikon Ti Eclipse) with a Nikon APO LWD 40×/1.15 NA WI water immersion objective (Figure S5A). Each sample was imaged at low laser power (1%), followed by an intense laser pulse (100% 5.4 mW power) for 5 s to bleach a small circular (5 μm diameter) and a 7 μm × 1.5 μm rectangular region of interest, ROI (Figure S5B). The time-dependent fluorescence signal was observed in the FITC (560 nm) and TRITC (595 nm) channels, respectively, and normalized to the intensity of the unbleached regions surrounding the ROIs. Steric interactions between dye molecules lead to a difference in diffusivity through the collagen matrix and the free solution,[34] necessitating the measurement of the free diffusion, D_0, of the dyes. The ratio of diffusivity within a sheet to that in free solution (D/D_0) is shown in Figure S5C. There were N = 4 replicates for each experimental condition.

2.12. Water Permeability Assay. The permeability coefficient of water through an aligned collagen sheet was measured using a pressure-driven filtration setup. The setup consisted of a vacuum filtration assembly (funnel capacity 15 mm, membrane diameter 25 mm, neck diameter 27 mm, Sigma-Aldrich), a vacuum-regulating valve (McMaster Carr, Elmhurst, IL, U.S.A.), and a pressure gauge to actively control and monitor the pressure difference applied across the sheet. Briefly, collagen sheets were cut into 12 mm diameter circular pieces using a carbon dioxide laser (laser power setting: 2% of 40 W, speed setting: 50%; model 8000, Epilog Mini Laser, Mississauga, ON,
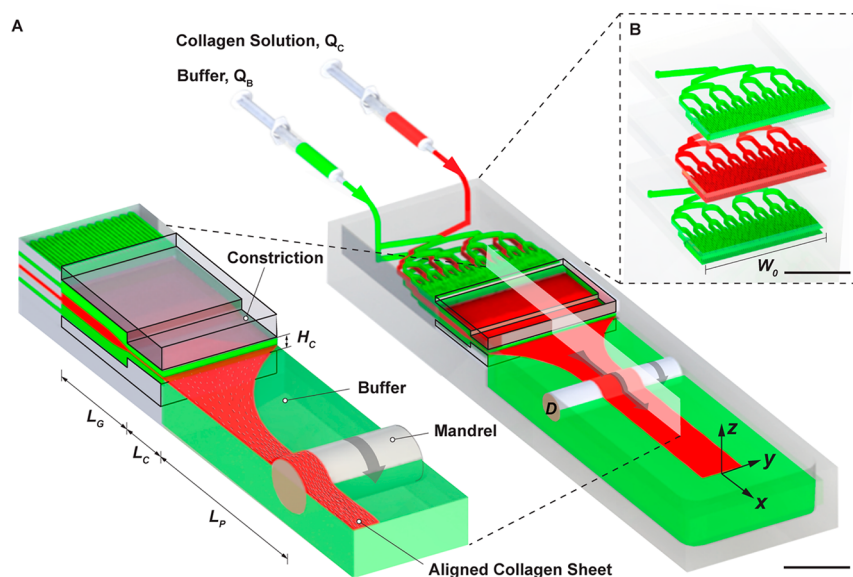
Figure 1. Schematic of a biofabrication approach for continuous formation of ultrathin collagen sheets. Collagen (red) and buffer solutions (green) are delivered to a three-layered microfluidic device. A collagen sheet emerges at the device exit, hydrodynamically focused between buffer solutions, and guided through a geometric constriction. An emerging collagen sheet undergoes fibrillogenesis and further strained by passing over a rotating mandrel (velocity V_P). Continued incubation, washing and drying results in the production of multicentimeter-wide, meter-long, ultrathin collagen sheets. (A) Enlarged view of hydrodynamic focusing of a collagen solution by a geometric flow constriction (L_G = 2 mm, L_C = 7.6 mm, H_C = 1 mm) with pH-induced fibril formation. Fibril alignment within the collagen sheet is due to both shear forces induced by solution flow through the geometric constriction, as well as strain imposed on the generated sheet by a downstream (L_P = 55 mm) mandrel (diameter D = 12.7 mm). (B) Schematic illustration of a three-layered microfluidic device containing hierarchical microchannel networks of width W_0 = 35 mm at the exit. Scale bars (A and B) 10 mm.

Canada). The circular sheet was placed on the filtration assembly membrane, and the area unoccupied by the sheet was sealed with a gasket material (Sticky Silicone Gel, McMaster Carr) to ensure water only permeated across the sheet. The permeability coefficient was evaluated based on the time required for 15 mL of water to permeate across a sheet, according to equation[35]

$$k = Q\delta\mu/\Delta PA \tag{3}$$

where Q, δ, μ, ΔP, and A represent the volumetric flow rate, the aligned collagen sheet thickness, the viscosity of water, the pressure difference across the sheet, and the filtration area, respectively. There were N = 5 replicates for each experimental condition.

2.13. Cell Culture. All primary cells were purchased from Lonza (Walkersville, MD), and cultured at 37 °C and 5% CO_2. Human aortic smooth muscle cells (vSMCs) were cultured in medium consisting of high-glucose Dulbecco's modified Eagle's medium (DMEM) with serum (20%), insulin (0.13 U/mL), basic fibroblast growth factor (bFGF; 10 ng/mL), epidermal growth factor (EGF; 0.5 ng/mL), penicillin G (10,000 U/mL), copper sulfate (3 ng/mL), L-proline (50 ng/mL), L-alanine (40 ng/mL), and glycine (50 ng/mL) and used prior to passage 9. Human aortic endothelial cells (HAECs) were cultured in fully supplemented EGM-2 (Lonza, Walkersville, MD) and used prior to passage 9.

2.14. Cell Alignment Quantification. Collagen sheets were sterilized in ethanol solution (70%) containing an antibiotic/antimycotic solution (1%) for 30 min and then rinsed with three washes of PBS pH 7.4. vSMCs were trypsinized and seeded at a concentration of 40,000 cells/cm². Cells were allowed to adhere for 4 h and additional media was then added to the tissue culture well. After appropriate culture times, samples were stained with calcein AM (2 μM) and ethidium homodimer (4 μM) and imaged with a Leica SP5 X inverted confocal microscope (Wetzlar, Germany). Alignment was quantified using a fast Fourier transform function in ImageJ on an intensity threshold based binarized image, utilizing the radial summing profile in 5° increments. These data were then plotted and FWHM calculated. Cell shape index (CSI), a dimensionless measurement of cell morphology

$$CSI = P^2/4\pi A \tag{4}$$

was quantified using the open source CellProfiler image analysis software (https://cellprofiler.org) to determine the area (A) and the perimeter (P) of each cell, CSI was calculated as previously described.[36]

2.15. Immunofluorescent Staining. Collagen sheets were sterilized and human aortic endothelial cells (HAECs) were trypsinized and seeded at density of 100,000 cells/cm² in fully supplemented EGM-2 onto collagen sheets or into individual wells of 6-well plates and allowed to adhere for 48 h. Medium was then replaced with fully supplemented EGM-2 without serum for 24 h to achieve a quiescent phenotype. Positive control samples were treated with TNF-α (100 ng/mL in EGM-2) for 4 h prior to fixation and staining. Samples were fixed in buffered formalin (10%) for 20 min at 4 °C, then washed three times with PBS pH 7.4 for 5 min each. Permeabilization was completed with a 5 min incubation in Triton X-100 (0.3%) in PBS and samples were then washed three times with Triton X-100 (0.1%) in PBS (PBS-T) for 5 min each. Non-specific binding was blocked for 30 min at room temperature with a solution of Triton X-100 (0.1%) in PBS containing BSA (2%, Abdil) and then washed three times with PBS-T for 5 min each. Primary antibodies were utilized at 1:50 dilutions (ICAM-1, VCAM-1 (Abcam)). Samples were also stained for F-actin (1:40 from a 6.6 μM stock solution, Life Technologies) for 1 h following standard protocol. Samples were mounted with Prolong Antifade containing DAPI (Life Technologies) and stored at 4 °C until imaging on a Leica SP5 X inverted confocal microscope (Wetzlar, Germany).

2.16. RT-PCR Analysis. HAECs were seeded onto collagen sheets or individual wells of 6-well plates, as described above. Following exposure to TNF-α, cells were washed three times with PBS, and RNA was isolated using the RNeasy Mini Kit (Qiagen).[37,38] RNA quantification was performed using a NanoDrop ND-1000 Spectrophotometer (Thermo Fisher Scientific) and reverse transcription was performed using 0.5 μg of total RNA per sample with the High Capacity cDNA Reverse Transcription Kit (Applied Biosystems) using the GeneAmp PCR System 9600 (PerkinElmer).
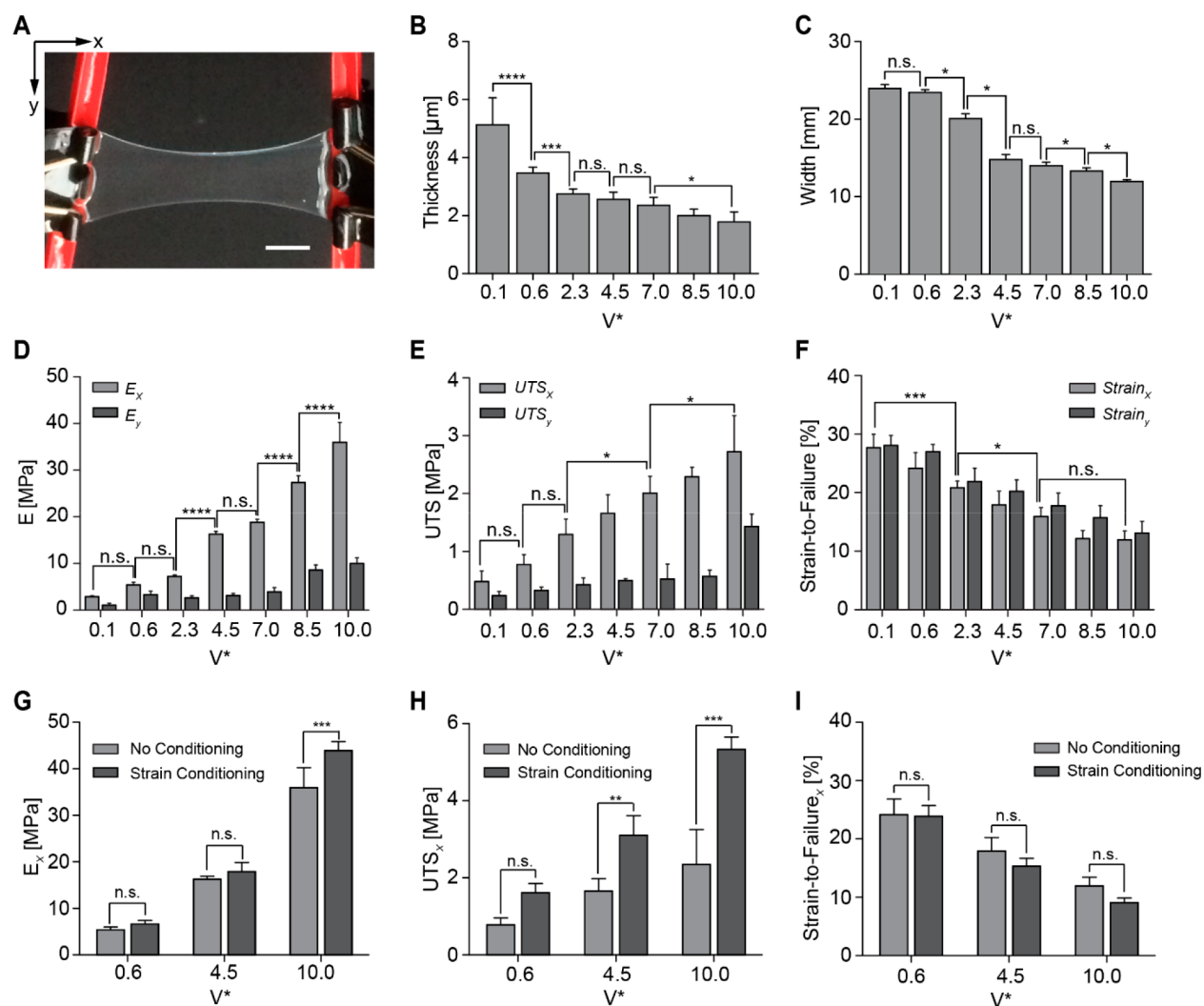
Figure 2. Macro and microscale properties of ultrathin collagen sheets. (A) Photograph of a collagen sheet produced at $V^* = 4.5$. Sheet thickness (B) and width (C), as well as elastic modulus (D), ultimate tensile strength (E), and strain-to-failure (F), in axial, x, and transverse, y, directions for collagen sheets produced as a function of varying V^*. Tensile properties, including E_x (G), UTS_x (H), and strain-to-failure$_x$ (I), were measured for collagen sheets in the axial, x, direction with or without further (15%) strain conditioning. Scale bar (A) 10 mm. $N = 8$ for all measurements; $*p < 0.05$, $**p < 0.01$, $*** p < 0.001$, $**** p < 0.0001$.

qPCR was performed using the ViiA 7 Real-Time PCR System (Thermo Fisher Scientific) and accompanying software. TaqMan Universal PCR Master Mix (Applied Biosystems) and TaqMan probes were used for ICAM1 (Hs00164932_m1) and VCAM1 (Hs01003372_m1), as markers of activation, and RPLP0 (Hs00420895_gH), as a housekeeping gene. Cycle threshold (Ct) raw data values were analyzed using the delta−delta Ct method to determine whether there were changes in markers of endothelial cell activation between groups.

2.17. Thin Film Contractility Assay. vSMC contractility was measured on aligned ($V^* = 4.5$) and weakly aligned ($V^* = 0.6$) collagen sheets using a thin film-based contractility assay. Briefly, elastic cantilevers were fabricated by manually dissecting collagen sheets into rectangular cantilevers that were 7 mm long (x - direction) and 3 mm wide (y - direction). One end of the cantilever was fixed using PDMS prior to seeding with vSMC (40,000 cells/cm^2). Samples were cultured in fully supplemented media at 37 °C for 48 h, followed by 24 h of culture in serum-free media. During the contractility assay, samples were incubated in Tyrode's solution (137 mM NaCl, 5.4 mM KCl, 1.2 mM MgCl$_2$, 20 mM HEPES, pH 7.4) at 37 °C. After peeling, the cantilevers were exposed to a vasoconstrictor (endothelin-1, 100 nM) at $t = 5$ min, followed by a rho-kinase inhibitor (HA-1077, 100 μM) at $t = 20$ min. The deflection of the free edge of the cantilever

was tracked using a stereoscope coupled to a National Instrument LabVIEW board. A MATLAB code and ImageJ were used to analyze recorded videos and reduce background noise. Active stress, basal tone, and residual stress were calculated using a previously published model.[39,40] By knowing the Young's modulus, thickness, and length of the collagen cantilevers, as well as the measured deflection, the tension can be calculated throughout the experiment. In particular, active stress and basal tone are defined by the difference in tension prior to treatment ($t = 0$) and after endothelin-1 and HA-1077 exposure, respectively. Residual stress is equal to the tension maintained on the cantilever after HA-1077 treatment.

2.18. Statistics. Mean and standard deviation were obtained for all measurements with a minimum of at least $n = 8$ for each condition. Comparisons were made using ANOVA for multiple comparisons, with Tukey post hoc analysis for parametric data, and Kruskal−Wallis for nonparametric data. Values of $p < 0.05$ were marked with $*$, $p < 0.01$ with $**$, $p < 0.001$ with $***$, and $p < 0.0001$ with $****$.

3. RESULTS AND DISCUSSION

3.1. Approach for Aligned Collagen Sheet Formation. Here, we report a microfluidic strategy for the rapid and continuous formation of multidimensional collagen structures.
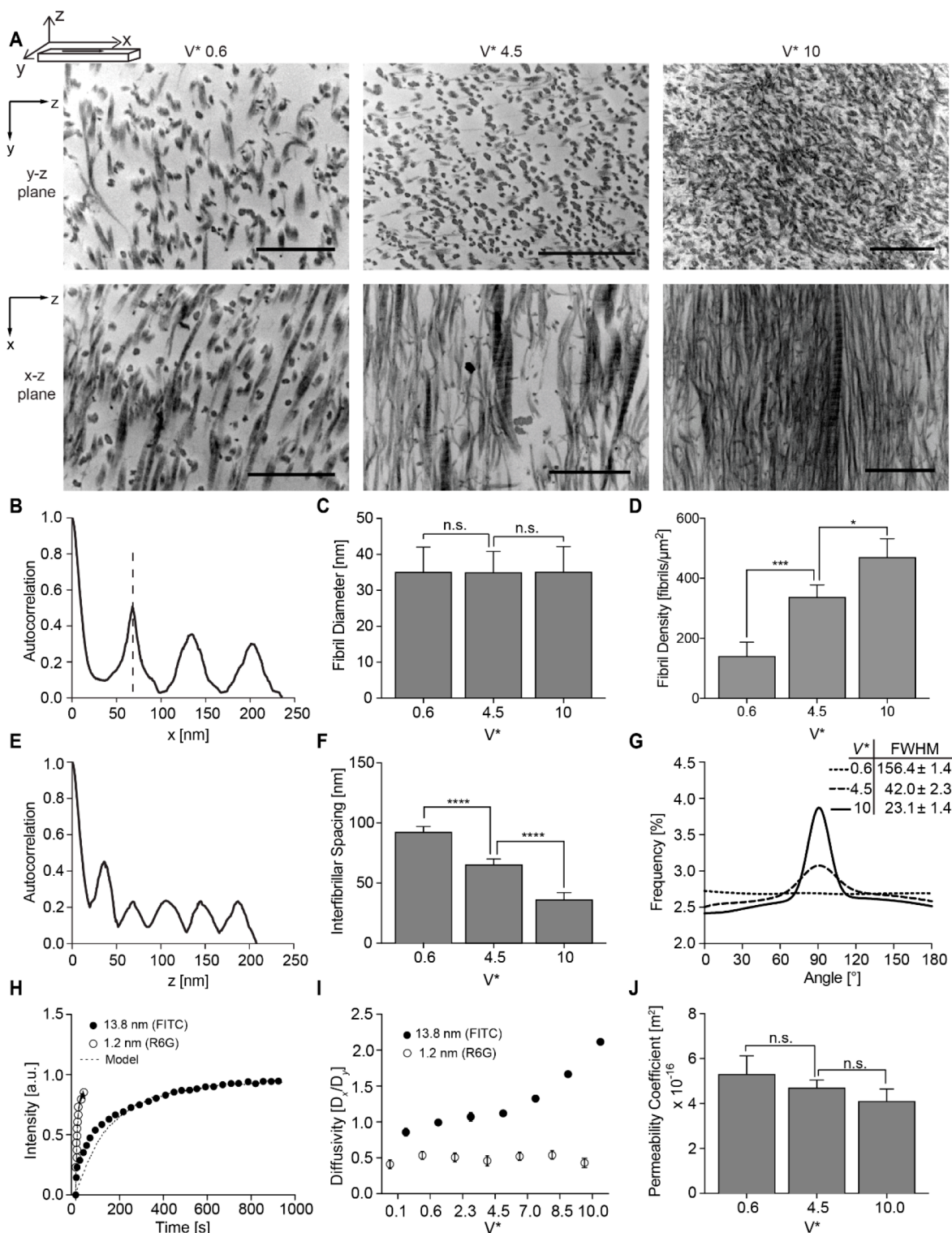
Figure 3. Nanostructure and molecular features of collagen sheets. (A) TEM images of collagen sheets produced at $V^* = 0.6$, 4.5, and 10 in $(y-z)$ and $(x-z)$ planes. (B) Autocorrelation of TEM images for sheets produced at V^* 10 in $(x-z)$ plane revealed collagen fibril D-periodic banding of ~67 nm. (C) Collagen fibril diameter was constant, while (D) fibril packing density increased with V^*. (E) Representative autocorrelation function of TEM images in $(x-z)$ plane to determine center-to-center fibril spacing for a collagen sheet produced at $V^* = 10$. (F) Fibril spacing decreased from 93 to 36 nm with increasing V^*. (G) Fibril alignment was obtained from the spectral analysis of TEM images in the $(x-z)$ plane of sheets generated at $V^* = 0.6$, 4.5, and 10. (H) Representative fluorescence recovery curves for a 5 μm diameter circular bleached region determined in the $(x-y)$ plane to assess in-plane diffusion of R6G (o) and FITC (●) within collagen sheets ($V^* = 10$). Experimental data were fitted to a model (dashed line) for determining diffusion times and coefficients. (I) Measured in-plane diffusivity, D_x/D_y. (J) Measured permeability coefficient for water transport through collagen sheets at a 3.4 kPa pressure difference. Scale bar (A) 500 nm. $N = 8$ for all measurements; *$p < 0.05$, ***$p < 0.001$, ****$p < 0.0001$.

Figure 1A illustrates our strategy for preparing ultrathin, handleable collagen sheets with precise control over collagen alignment and compaction. A microfluidic device distributes a collagen solution uniformly in the lateral direction to form, at its exit, a multicentimeter-wide collagen layer that is hydrodynamically focused while passing through a downstream constriction. A floating collagen sheet with tunable dimensions and anisotropic tensile and transport properties is obtained by the combined effects of fibrillogenesis and macromolecular crowding, and the strain applied by passing over a rotating mandrel.

Briefly, an acidic type I collagen (pH 2) solution is delivered at flow rate Q_C to the center layer of a three-layered microfluidic device [see ref 30 or Figure S1 for the microfluidic channel pattern]. A flow focusing buffer (FFB, pH 8) solution is supplied at flow rate Q_B to the device top and bottom layers (Figure 1B). A centimeter-wide collagen layer leaves the device and is hydrodynamically focused[41] between the two buffer solutions at a shear rate on the order of 10^1 s^{-1} while passing through a downstream constriction. See Figure S2 for a schematic and photograph of the microfluidic fabrication system.

As the collagen solution approaches its isoelectric point (pH 7.4),[42] the reduced electrostatic repulsion between the positively charged collagen molecules and dominant hydrophobic interactions favor nucleation and growth of fibrils via pH-triggered fibrillogenesis with self-assembly of collagen molecules into anisotropic fibrils. In addition, polyethylene glycol (PEG), a molecular crowding agent and key component in the FFB solution, creates a hypertonic environment, which causes the expulsion of water from the collagen layer, resulting in fibrillar compaction[16] with the generation of a free-floating collagen sheet. The sheet is strained by a rotating mandrel over which it passes, inducing fibril alignment along the extrusion direction, x. In some cases, referred to as "strain conditioning", we applied strain after sheet formation. To complete collagen fibril growth, as-produced sheets were incubated at 37 °C for 48 h in a buffer system to further promote fibrillogenesis,[15] and subsequently washed and dried to increase compaction. The combined effects of pH induced fibrillogenesis, shear, strain, macromolecular crowding, and evaporation produces ultrathin, aligned collagen sheets.

3.2. Dimensions and Tensile Properties of Ultrathin Collagen Sheets.
Figure 2A shows a photograph of the extruded collagen sheet. Collagen sheets of varying thickness and width were obtained by altering the mandrel velocity (2.3–23 mm/s) at fixed flow rates of Q_C = 400 μL/min and Q_B = 4000 μL/min. The mean thickness, δ, of fully hydrated collagen sheets decreased from 5.2 ± 0.9 μm to 1.9 ± 0.3 μm as V^* increased from 0.1 to 10 (Figure 2B). The capacity to generate ultrathin, yet handleable collagen sheets will facilitate structural mimicry of important tissues, such as cornea and blood vessels, and provides the flexibility of including intervening layers of additional extracellular matrix components, such as proteoglycans and growth factors or elastin, in the fabrication of cell populated multilayer structures, while minimizing the total thickness of the structure. Similarly, with increasing V^*, sheet width decreased from that at the exit section of the microfluidic device, W_0 = 35.0 mm to 12.0 ± 0.2 mm (V^* 10) (Figure 2C). After washing, Fourier-transform infrared (FTIR) spectroscopy confirmed the absence of a peak at 1100 cm^{-1}, indicative of the complete removal of PEG in the prepared collagen sheets (Figure S3). Sheets exhibited

anisotropic tensile properties in the extrusion direction, x, and the lateral direction, y. Sheet elastic moduli E_x of 2.9–35.9 MPa and E_y of 1.5–10.0 MPa (Figure 2D), were associated with ultimate tensile strengths UTS_x of 0.5–2.7 MPa and UTS_y of 0.2–1.4 MPa (Figure 2E) and increased with increasing V^*. Strain-to-failure in the extrusion direction, 27.7–12.0%, and the lateral direction, 28.1–13.1%, (Figure 2F), decreased with increasing V^*. We attribute the increase in E and UTS to increased fibril compaction and alignment. Strain conditioning of collagen sheets by 15% further increased tensile properties for those sheets produced at high V^* (see Figure S4 for experimental setup). Sheets produced at V^* = 10 and subsequently subjected to 15% strain, displayed E_x = 44 MPa (Figure 2G), UTS_x = 5.3 MPa (Figure 2H), and a strain-to-failure in the alignment direction of 9.1% (Figure 2I). We attribute the augmentation of mechanical properties to a further increase in fibril alignment during continuous straining. Collagen sheets were produced using a 5 mg/mL collagen solution. While not systematically evaluated, sheet nanoscale structure and mechanical behavior would likely be influenced by solution concentration. Using lower concentrations is expected to extend the gelation time scale and affect the consistency of extrusion and uniformity of the obtained sheets. Extruding at higher concentration is expected to shorten the gelation time scale and increase the elastic modulus and UTS values of the aligned collagen sheets and reduce the strain-to-failure.[43]

3.3. Strain Increases Fibril Alignment and Compaction and Inhibits Molecular Transport.
Electron microscopy was used to evaluate the nanoscale properties of the fabricated sheets. Figure 3A shows transmission electron microscopy (TEM) images obtained in the (y–z) and the (x–z) planes, for V^* = 0.6, 4.5, and 10. The increase in fibrillar alignment and compaction is evident from these images. TEM images obtained in the (x–z) plane and the related autocorrelation function evaluated in the x-direction, as an ensemble average over all z positions (Figure 3B), confirmed the presence of a periodic 67 nm D-banding pattern typical of mature collagen fibrils. As shown in Figure 3C, fibrils were produced with an average diameter of 35.1 ± 6.5 nm and was comparable to that reported in the literature.[15,18] The fibril packing density increased from 141 ± 46 to 470 ± 61 fibrils/μm^2 for V^* = 0.6 and 10, respectively (Figure 3D). Autocorrelating the TEM images in the (x–z) plane along the z direction, as an ensemble average over all x positions (Figure 3E), provided a measure of the center-to-center interfibrillar spacing. Spacing decreased from 92.6 ± 4.5 to 36.3 ± 5.8 nm for V^* = 0.6 and 10, respectively (Figure 3F). Fast Fourier transform (FFT) of TEM images in the (x–z) plane, reveals an increase in fibril alignment in the x direction with increasing V^* (Figure 3G). Approximately 70% of fibrils were aligned within 10° of one another and 40% of fibrils within 5°.

Molecular transport across aligned collagen sheets was evaluated using fluorescence recovery after photobleaching (FRAP). Measurements conducted in the (x–y) plane for a sheet produced at V^* = 10 revealed the directional dependence of molecular transport as a function of solute molecular size. Figure 3H illustrates fluorescence recovery curves for Rhodamine (R6G, M_W 479 g/mol, hydrodynamic diameter 1.2 nm) and FITC-dextran (M_W 150 000 g/mol, hydrodynamic diameter 13.8 nm) within a sheet prepared at V^* = 10, which were in agreement with a stochastic model developed by
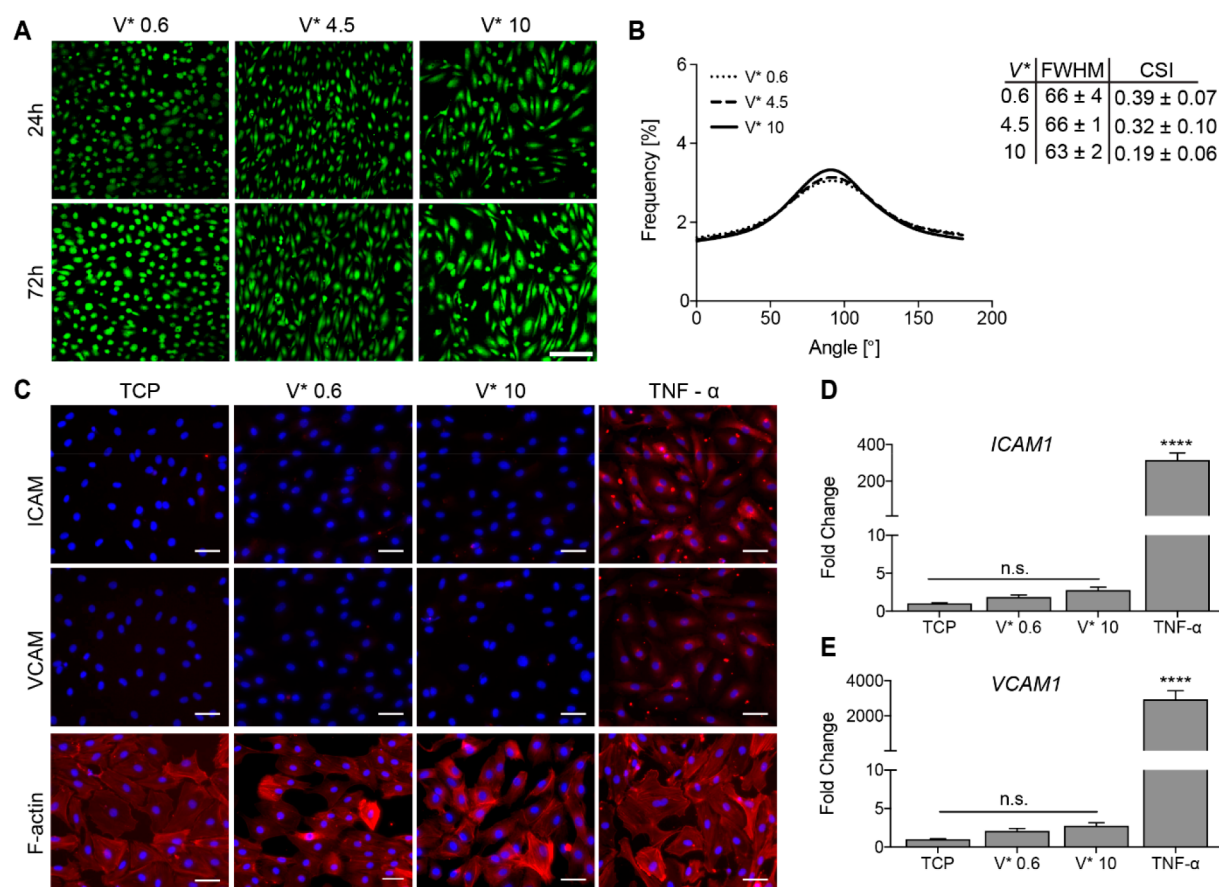
Figure 4. Collagen fibril alignment influences endothelial cell morphology without promoting cellular activation. (A) Human aortic ECs were cultured on collagen sheets produced at $V^* = 0.6$, 4.5, and 10 over 24 and 72 h. (B) Quantification of EC alignment cultured on collagen sheets produced at $V^* = 0.6$, 4.5, and 10 by FFT image analysis and corresponding fwhm and cell shape indices (CSI). (C) Immunofluorescent staining of F-actin and pro-inflammatory markers, ICAM-1 and VCAM-1 (TCP = tissue culture plastic). RT-PCR of (D) ICAM-1 and (E) VCAM-1 expression (mean ± SEM). Scale bars (A) 50 μm and (C) 50 μm. $N = 8$ for all measurements; ****$p < 0.0001$.

Axelrod et al.[44] Diffusivity was calculated using the relation $D = \omega^2/4\tau_D$ where ω is the radius of the Gaussian bleaching profile and τ_D is a characteristic diffusion time. For a circular bleached region, τ_D was 80 and 932 s for R6G and FITC-dextran, respectively, consistent with a fluorescence recovery that was 11.7 times faster for R6G than for FITC-dextran. We attribute this difference to size-exclusion of FITC-dextran molecules, due to their hydrodynamic diameter being comparable to the average gap between neighboring fibrils of 1.2 nm, and 11.5-fold larger than the hydrodynamic diameter of R6G. The effect of anisotropic fibril alignment on molecular transport was evaluated in the $(x-y)$ plane within a rectangular bleached region (see Figure S5 for details). Figure 3I summarizes the ratio of the diffusion coefficients determined in axial and transverse directions, D_x/D_y, as a function of V^*. FITC-dextran molecules diffuse preferentially along the x-direction. This effect became more pronounced with increasing V^*, due to an increase in molecular alignment and compaction. At $V^* = 10$, the size exclusion effect was evident for FITC-dextran, while the smaller R6G molecules isotropically diffused in the x and the y directions, regardless of V^*. Figure 3J demonstrates the permeability of water across collagen sheets prepared at varying V^*. A decrease in interfibril spacing was associated with a non-significant reduction in water permeability with measured permeability coefficients of 10^{-16} m^2; comparable to reports for type I collagen scaffolds.[45]

3.4. Collagen Fibril Alignment Induces Cellular Alignment and Coordinated Tissue Responses.

Human aortic endothelial cells (ECs) were cultured on collagen sheets for 72 h to evaluate the effect of fibrillar alignment and compaction on EC morphology and related cell behavior (Figure 4A). We investigated collagen sheets extruded at $V^* = 0.6$, 4.5, and 10 in order to investigate cellular properties at a wide range of alignment (unaligned, semialigned, and highly aligned). However, no significant differences in cell organization or orientation were observed. Nonetheless, ECs exhibited a more rounded morphology, as determined by a cell shape index (CSI) of 0.39 ± 0.07, when cultured on sheets with limited fibril alignment ($V^* = 0.6$), as compared to those cells grown on highly anisotropic ($V^* = 10$) collagen sheets with an observed CSI of 0.19 ± 0.06 (Figure 4B). Minimal expression of inflammatory cell surface markers, ICAM-1 and VCAM-1, was observed (Figure 4C), and comparable to cells grown under quiescent culture conditions on tissue culture plastic. RT-PCR further confirmed that collagen fibril alignment did not influence expression of ICAM-1 or VCAM-1, whereas exposure to TNF-α induced a 300- and 3000-fold increase in gene expression, respectively (Figure 4D,E).

As anticipated, collagen fibril alignment had a significant impact on vascular smooth muscle cell (vSMC) organization. vSMCs cultured on minimally aligned (V^* 0.6) collagen sheets displayed little measurable alignment, while a high degree of
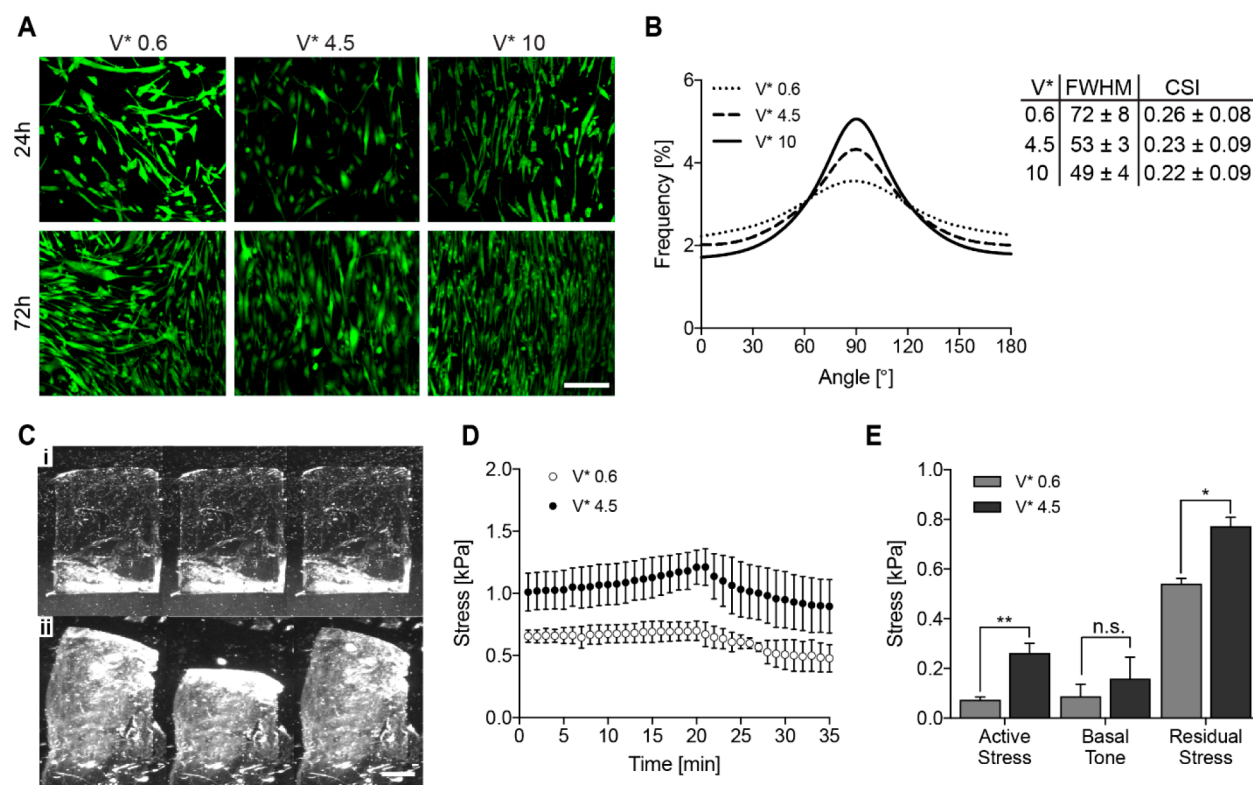
Figure 5. Collagen fibril alignment influences smooth muscle cell orientation and contractile responses. (A) Human aortic vSMCs cultured on collagen sheets produced at $V^* = 0.6$, 4.5, and 10 over 24 and 72 h. (B) Quantification of alignment of vSMCs cultured on collagen sheets produced at V^* 0.6, 4.5, and 10 by FFT image analysis and corresponding FWHM and cell shape indices (CSI). (C) Vasomotor responses of vSMCs on collagen sheets produced at V^* 0.6 (i) and 4.5 (ii) with associated average time traces of generated stress (D). Samples were stimulated with endothelin 1 (100 nM) at 5 min and HA-1077 (100 μM) at 20 min with measurement of (E) active stress and basal tone, respectively. Scale bars (A) 50 μm and (C) 1 mm. $N = 8$ for all measurements; $*p < 0.05$, $**p < 0.01$.

vSMC orientation was observed on sheets fabricated at $V^* = 4.5$ and 10 in the direction of aligned collagen fibrils (Figure 5A). When quantified, the full width at half-maximum for FFT generated plots varied from $72 \pm 8°$ to $49 \pm 4°$ for $V^* = 0.6$ and 10, respectively. The associated CSI did not vary significantly between conditions (Figure 5B). vSMC alignment in the direction of fibril orientation had a corresponding effect on coordinated contractile responses, which was evaluated using an approach similar to that described for synthetic cantilevers.[39,40] vSMC-seeded collagen cantilevers were exposed at $t = 5$ min to a vasoconstrictor, endothelin-1 (100 nM), followed by a rho-kinase inhibitor (HA-1077, 100 μM) at $t = 20$ min. Representative images of endothelin-1 induced vasoconstriction and HA-1077 induced vasorelaxation are shown in Figure 5C. Quantification of the stress generated by cell seeded cantilevers revealed that coordinated vasoconstrictive and vasorelaxation responses were only observed when vSMCs were cultured on sheets composed of highly aligned collagen fibrils with associated induction of vSMC alignment (Figure 5D). Higher absolute values of contractile stress and residual stress were characteristic of coherently aligned cell-sheet structures (Figure 5E). Cell-seeded cantilevers prepared from highly aligned ($V^* = 10$) collagen sheets exhibited a level of contractility that surpassed the limits of the employed assay, and thus were not included.

4. CONCLUSIONS

We have developed a new biofabrication strategy for the continuous formation of ultrathin, multicentimeter wide collagen sheets (width-to-thickness ratio up to 5000) of extended lengths (>230 mm) with tunable degrees of fibril compaction and orientation. The combination of hydrodynamic focusing, strain-induced pulling, osmotic gradient induction, and evaporative drying formed anisotropic aligned collagen sheets with the extent of fibril alignment and density consistent throughout the entire structure. This approach provides an unprecedented ability to rapidly fabricate sheets composed of collagen, presumably with other ECM proteins as desired, that are strong yet ultrathin. Sheets produced in this manner are at least 10−20 fold thinner than prior approaches used to fabricate free-standing collagen sheets and can be readily applied for direct use or in the structural mimicry of native tissues. Significantly, the described microfluidic scheme affords extracellular matrix-based sheets that are 20-fold thinner than those produced by the decellularization of cell sheets that have been produced over a culture period of 6 or more weeks.[46,47] Large aspect-ratio collagen sheets with dimensions that ranged from 1.9−5 μm in thickness and 12−24 mm in width were continuously produced. The degree of alignment and compaction of the collagen fibrils was controlled, with up to 40% of fibrils aligned within 5° of one another. As a result, highly aligned collagen sheets achieved mechanical properties comparable with many tissues in the body, with elastic moduli of 3−36 MPa, ultimate tensile strengths of 0.5−2.5 MPa, and strain-to-failure of 12−28%. In addition, the presence of D-periodic banding of ∼ 67 nm typical of native collagen fibrils was consistently observed. Cell behavior was responsive to induced fibril organization, with

endothelial cells exhibiting characteristic morphological changes and vascular smooth muscle cells displaying preferential alignment in the direction of collagen fibrils with coordinated vasomotor responses. We believe that the scalable and free-standing production of handleable, anisotropically aligned ultrathin collagen sheets of biologically relevant composition, architecture, dimensions, and mechanical properties will greatly facilitate the engineering of a variety of load bearing and cell containing multilamellar structures composed of fibrillar collagen and other ECM proteins, such as tendons, fascia, cornea, esophagus, intestine, bladder, ureter, urethra, myocardium, heart and venous valves, and blood vessels.

■ ASSOCIATED CONTENT

ⓈⒾ Supporting Information

The Supporting Information is available free of charge at https://pubs.acs.org/doi/10.1021/acsbiomaterials.0c321.

> Details on the microfluidic device design, microfluidic extrusion system, strain conditioning of collagen sheets, fluorescence recovery after photobleaching (FRAP) setup, and FTIR spectrum of aligned collagen sheets are shown (PDF)

■ AUTHOR INFORMATION

Corresponding Authors

Axel Günther − *Department of Mechanical and Industrial Engineering and Institute of Biomaterials and Biomedical Engineering, University of Toronto, Toronto, Ontario M5S3G8, Canada;* ⓘ orcid.org/0000-0002-0592-2261; Phone: +1 416-978-1282; Email: guenther@mie.utoronto.ca

Elliot L. Chaikof − *Division of Health Sciences and Technology, Massachusetts Institute of Technology, Cambridge, Massachusetts 02139, United States; Department of Surgery, Beth Israel Deaconess Medical Center, Boston, Massachusetts 02115, United States; Wyss Institute for Biologically Inspired Engineering of Harvard University, Harvard University, Cambridge, Massachusetts 02138, United States;* Phone: +1 617-632-9581; Email: echaikof@bidmc.harvard.edu

Authors

Shashi Malladi − *Department of Mechanical and Industrial Engineering, University of Toronto, Toronto, Ontario M5S3G8, Canada*

David Miranda-Nieves − *Division of Health Sciences and Technology, Massachusetts Institute of Technology, Cambridge, Massachusetts 02139, United States; Department of Surgery, Beth Israel Deaconess Medical Center, Boston, Massachusetts 02115, United States; Wyss Institute for Biologically Inspired Engineering of Harvard University, Harvard University, Cambridge, Massachusetts 02138, United States*

Lian Leng − *Department of Mechanical and Industrial Engineering, University of Toronto, Toronto, Ontario M5S3G8, Canada*

Stephanie J. Grainger − *Department of Surgery, Beth Israel Deaconess Medical Center, Boston, Massachusetts 02115, United States*

Constantine Tarabanis − *Department of Surgery, Beth Israel Deaconess Medical Center, Boston, Massachusetts 02115, United States*

Alexander P. Nesmith − *Wyss Institute for Biologically Inspired Engineering of Harvard University, Harvard University, Cambridge, Massachusetts 02138, United States*

Revanth Kosaraju − *Department of Surgery, Beth Israel Deaconess Medical Center, Boston, Massachusetts 02115, United States*

Carolyn A. Haller − *Department of Surgery, Beth Israel Deaconess Medical Center, Boston, Massachusetts 02115, United States*

Kevin Kit Parker − *Wyss Institute for Biologically Inspired Engineering of Harvard University, Harvard University, Cambridge, Massachusetts 02138, United States;* ⓘ orcid.org/0000-0002-5968-7535

Complete contact information is available at:
https://pubs.acs.org/10.1021/acsbiomaterials.0c00321

Author Contributions

▽S.M. and D.M.-N. contributed equally.

Notes

The authors declare no competing financial interest.

■ ACKNOWLEDGMENTS

■ REFERENCES

(1) Fratzl, P.; Weinkamer, R. Nature's hierarchical materials. *Prog. Mater. Sci.* **2007**, *52* (8), 1263−1334.

(2) Fratzl, P. Collagen: Structure and Mechanics, an Introduction. In *Collagen: Structure and Mechanics*; Fratzl, P., Ed.; Springer US: Boston, MA, 2008; pp 1−13.

(3) Buehler, M. J. Nature designs tough collagen: explaining the nanostructure of collagen fibrils. *Proc. Natl. Acad. Sci. U. S. A.* **2006**, *103* (33), 12285−12290.

(4) Dyer, R. F.; Enna, C. D. Ultrastructural features of adult human tendon. *Cell Tissue Res.* **1976**, *168* (2), 247−259.

(5) Elliott, D. H. Structure and Function of Mammalian Tendon. *Biological Reviews* **1965**, *40* (3), 392−421.

(6) Maurice, D. M. The structure and transparency of the cornea. *J. Physiol.* **1957**, *136* (2), 263−286.

(7) Meek, K. M. Corneal collagen—its role in maintaining corneal shape and transparency. *Biophys. Rev.* **2009**, *1* (2), 83−93.

(8) Wagenseil, J. E.; Mecham, R. P. Vascular extracellular matrix and arterial mechanics. *Physiol. Rev.* **2009**, *89* (3), 957−989.

(9) Shadwick, R. E. Mechanical design in arteries. *J. Exp Biol.* **1999**, *202*, 3305−3313.

(10) Lee, A.; Hudson, A. R.; Shiwarski, D. J.; Tashman, J. W.; Hinton, T. J.; Yerneni, S.; Bliley, J. M.; Campbell, P. G.; Feinberg, A. W. 3D bioprinting of collagen to rebuild components of the human heart. *Science* **2019**, *365* (6452), 482−487.

(11) Rhee, S.; Puetzer, J. L.; Mason, B. N.; Reinhart-King, C. A.; Bonassar, L. J. 3D Bioprinting of Spatially Heterogeneous Collagen Constructs for Cartilage Tissue Engineering. *ACS Biomater. Sci. Eng.* **2016**, *2* (10), 1800−1805.

(12) Grigoryan, B.; Paulsen, S. J.; Corbett, D. C.; Sazer, D. W.; Fortin, C. L.; Zaita, A. J.; Greenfield, P. T.; Calafat, N. J.; Gounley, J. P.; Ta, A. H.; Johansson, F.; Randles, A.; Rosenkrantz, J. E.; Louis-Rosenberg, J. D.; Galie, P. A.; Stevens, K. R.; Miller, J. S. Multivascular networks and functional intravascular topologies within biocompatible hydrogels. *Science* **2019**, *364* (6439), 458−464.

(13) Weinberg, C. B.; Bell, E. A blood vessel model constructed from collagen and cultured vascular cells. *Science* **1986**, *231* (4736), 397−400.

(14) Kumar, V. A.; Caves, J. M.; Haller, C. A.; Dai, E.; Liu, L.; Grainger, S.; Chaikof, E. L. Acellular vascular grafts generated from collagen and elastin analogs. *Acta Biomater.* **2013**, *9* (9), 8067−8074.

(15) Caves, J. M.; Kumar, V. A.; Wen, J.; Cui, W.; Martinez, A.; Apkarian, R.; Coats, J. E.; Berland, K.; Chaikof, E. L. Fibrillogenesis in continuously spun synthetic collagen fiber. *J. Biomed. Mater. Res., Part B* **2009**, *93* (1), 24−38.

(16) Cavallaro, J. F.; Kemp, P. D.; Kraus, K. H. Collagen fabrics as biomaterials. *Biotechnol. Bioeng.* **1994**, *43* (8), 781−791.

(17) Pins, G. D.; Christiansen, D. L.; Patel, R.; Silver, F. H. Self-assembly of collagen fibers. Influence of fibrillar alignment and decorin on mechanical properties. *Biophys. J.* **1997**, *73* (4), 2164−2172.

(18) Caves, J. M.; Cui, W.; Wen, J.; Kumar, V. A.; Haller, C. A.; Chaikof, E. L. Elastin-like protein matrix reinforced with collagen microfibers for soft tissue repair. *Biomaterials* **2011**, *32* (23), 5371−5379.

(19) Haynl, C.; Hofmann, E.; Pawar, K.; Förster, S.; Scheibel, T. Microfluidics-Produced Collagen Fibers Show Extraordinary Mechanical Properties. *Nano Lett.* **2016**, *16* (9), 5917−5922.

(20) Cheng, X.; Gurkan, U. A.; Dehen, C. J.; Tate, M. P.; Hillhouse, H. W.; Simpson, G. J.; Akkus, O. An electrochemical fabrication process for the assembly of anisotropically oriented collagen bundles. *Biomaterials* **2008**, *29* (22), 3278−3288.

(21) Guo, C.; Kaufman, L. J. Flow and magnetic field induced collagen alignment. *Biomaterials* **2007**, *28* (6), 1105−1114.

(22) Lanfer, B.; Freudenberg, U.; Zimmermann, R.; Stamov, D.; Korber, V.; Werner, C. Aligned fibrillar collagen matrices obtained by shear flow deposition. *Biomaterials* **2008**, *29* (28), 3888−3895.

(23) Torbet, J.; Malbouyres, M.; Builles, N.; Justin, V.; Roulet, M.; Damour, O.; Oldberg, A.; Ruggiero, F.; Hulmes, D. J. Orthogonal scaffold of magnetically aligned collagen lamellae for corneal stroma reconstruction. *Biomaterials* **2007**, *28* (29), 4268−4276.

(24) Kumar, V. A.; Caves, J. M.; Haller, C. A.; Dai, E.; Liu, L.; Grainger, S.; Chaikof, E. L. Collagen-Based Substrates with Tunable Strength for Soft Tissue Engineering. *Biomater. Sci.* **2013**, *1* (11), 1193.

(25) Son, J.; Bang, M. S.; Park, J.-K. Hand-Maneuverable Collagen Sheet with Micropatterns for 3D Modular Tissue Engineering. *ACS Biomater. Sci. Eng.* **2019**, *5* (1), 339−345.

(26) Barrett, D. J.; Linley, M. D.; Best, S. M.; Cameron, R. E. Fabrication of free standing collagen membranes by pulsed-electrophoretic deposition. *Biofabrication* **2019**, *11* (4), No. 045017.

(27) Ajalloueian, F.; Nikogeorgos, N.; Ajalloueian, A.; Fossum, M.; Lee, S.; Chronakis, I. S. Compressed collagen constructs with optimized mechanical properties and cell interactions for tissue engineering applications. *Int. J. Biol. Macromol.* **2018**, *108*, 158−166.

(28) Brown, R. A.; Wiseman, M.; Chuo, C. B.; Cheema, U.; Nazhat, S. N. Ultrarapid Engineering of Biomimetic Materials and Tissues: Fabrication of Nano- and Microstructures by Plastic Compression. *Adv. Funct. Mater.* **2005**, *15* (11), 1762−1770.

(29) Silver, F. H.; Trelstad, R. L. Type I collagen in solution. Structure and properties of fibril fragments. *J. Biol. Chem.* **1980**, *255* (19), 9427−9433.

(30) Leng, L.; McAllister, A.; Zhang, B.; Radisic, M.; Günther, A. Mosaic Hydrogels: One-Step Formation of Multiscale Soft Materials. *Adv. Mater.* **2012**, *24* (27), 3650−3658.

(31) Unger, M. A.; Chou, H. P.; Thorsen, T.; Scherer, A.; Quake, S. R. Monolithic microfabricated valves and pumps by multilayer soft lithography. *Science* **2000**, *288* (5463), 113−116.

(32) Tremblay, D.; Cuerrier, C. M.; Andrzejewski, L.; O'Brien, E. R.; Pelling, A. E. A novel stretching platform for applications in cell and tissue mechanobiology. *J. Visualized Exp.* **2014**, No. 88, 51454 DOI: 10.3791/51454.

(33) Hakimi, N.; Cheng, R.; Leng, L.; Sotoudehfar, M.; Ba, P. Q.; Bakhtyar, N.; Amini-Nik, S.; Jeschke, M. G.; Günther, A. Handheld skin printer: in situ formation of planar biomaterials and tissues. *Lab Chip* **2018**, *18* (10), 1440−1451.

(34) Ekani-Nkodo, A.; Fygenson, D. K. Size exclusion and diffusion of fluoresceinated probes within collagen fibrils. *Phys. Rev. E: Stat. Phys., Plasmas, Fluids, Relat. Interdiscip. Top.* **2003**, *67* (2), No. 021909.

(35) O'Brien, F. J.; Harley, B. A.; Waller, M. A.; Yannas, I. V.; Gibson, L. J.; Prendergast, P. J. The effect of pore size on permeability and cell attachment in collagen scaffolds for tissue engineering. *Technol. Health Care* **2006**, *15* (1), 3−17.

(36) Levesque, M. J.; Liepsch, D.; Moravec, S.; Nerem, R. M. Correlation of endothelial cell shape and wall shear stress in a stenosed dog aorta. *Arteriosclerosis* **1986**, *6* (2), 220−229.

(37) Nan, B.; Lin, P.; Lumsden, A. B.; Yao, Q.; Chen, C. Effects of TNF-alpha and curcumin on the expression of thrombomodulin and endothelial protein C receptor in human endothelial cells. *Thromb. Res.* **2005**, *115* (5), 417−426.

(38) Tang, S.; Le-Ruppert, K. C.; Gabel, V. P. Expression of intercellular adhesion molecule-1 (ICAM-1) and vascular cell adhesion molecule-1 (VCAM-1) on proliferating vascular endothelial cells in diabetic epiretinal membranes. *Br. J. Ophthalmol.* **1994**, *78* (5), 370−376.

(39) Agarwal, A.; Farouz, Y.; Nesmith, A. P.; Deravi, L. F.; McCain, M. L.; Parker, K. K. Micropatterning Alginate Substrates for in vitro Cardiovascular Muscle on a Chip. *Adv. Funct. Mater.* **2013**, *23* (30), 3738−3746.

(40) Alford, P. W.; Nesmith, A. P.; Seywerd, J. N.; Grosberg, A.; Parker, K. K. Vascular smooth muscle contractility depends on cell shape. *Integr Biol. (Camb)* **2011**, *3* (11), 1063−1070.

(41) Knight, J. B.; Vishwanath, A.; Brody, J. P.; Austin, R. H. Hydrodynamic Focusing on a Silicon Chip: Mixing Nanoliters in Microseconds. *Phys. Rev. Lett.* **1998**, *80* (17), 3863−3866.

(42) Highberger, J. H. The Isoelectric Point of Collagen. *J. Am. Chem. Soc.* **1939**, *61* (9), 2302−2303.

(43) Zhu, J.; Kaufman, L. J. Collagen I self-assembly: revealing the developing structures that generate turbidity. *Biophys. J.* **2014**, *106* (8), 1822−1831.

(44) Axelrod, D.; Koppel, D. E.; Schlessinger, J.; Elson, E.; Webb, W. W. Mobility measurement by analysis of fluorescence photobleaching recovery kinetics. *Biophys. J.* **1976**, *16* (9), 1055−1069.

(45) Ramanujan, S.; Pluen, A.; McKee, T. D.; Brown, E. B.; Boucher, Y.; Jain, R. K. Diffusion and convection in collagen gels: implications for transport in the tumor interstitium. *Biophys. J.* **2002**, *83* (3), 1650−1660.

(46) L'Heureux, N.; Paquet, S.; Labbe, R.; Germain, L.; Auger, F. A. A completely biological tissue-engineered human blood vessel. *FASEB J.* **1998**, *12* (1), 47−56.

(47) L'Heureux, N.; Dusserre, N.; Konig, G.; Victor, B.; Keire, P.; Wight, T. N.; Chronos, N. A.; Kyles, A. E.; Gregory, C. R.; Hoyt, G.; Robbins, R. C.; McAllister, T. N. Human tissue-engineered blood vessels for adult arterial revascularization. *Nat. Med.* **2006**, *12* (3), 361−365.